Journal of
Marine Science and Engineering

Article

Research on the Transport of Typical Pollutants in the Yellow Sea with Flow and Wind Fields

Nan Wang [1], Ruichen Cao [1,*], Xianqing Lv [1] and Honghua Shi [2,3,*]

[1] Frontier Science Center for Deep Ocean Multispheres and Earth System (FDOMES), Physical Oceanography Laboratory, Ocean University of China, Qingdao 266100, China; wn4858@stu.ouc.edu.cn (N.W.); xqinglv@ouc.edu.cn (X.L.)
[2] First Institute of Oceanography, Ministry of Natural Resources, Qingdao 266061, China
[3] Laoshan Laboratory, Qingdao 266237, China
* Correspondence: crc@stu.ouc.edu.cn (R.C.); shihonghua@fio.org.cn (H.S.)

Abstract: In this study, we developed a transport model for typical pollutants in the Yellow Sea using the Lagrangian particle tracking method to analyze the trajectories of fish feed, a common pollutant in the Yellow Sea. The model incorporates the influence of ocean currents and surface winds on pollutant transport and utilizes a series of numerical experiments to simulate pollutant transport. Through statistical analysis of the numerical experiment results, we identified characteristic circles that represent the pollutant distribution patterns. Furthermore, based on the current and wind information within these characteristic circles, we derived an empirical formula to describe pollutant distribution. This formula enables us to predict the spatial distribution of pollutants using available current and wind data. Using this empirical formula, we designed an effective path to avoid pollutant contamination. This approach not only optimizes the utilization of computational resources within the study area but also contributes to the rational planning of navigation routes for aquaculture vessels. Overall, our study provides valuable insights into the transport behavior of fish feed pollutants in the Yellow Sea. The establishment of the empirical formula and the design of effective routes to avoid pollution contribute to the efficient management of pollution and facilitate the planning of marine activities in the region.

Keywords: Yellow Sea; fish feed; Lagrangian particle tracking; pollutant transport; pollution management

check for updates

Citation: Wang, N.; Cao, R.; Lv, X.; Shi, H. Research on the Transport of Typical Pollutants in the Yellow Sea with Flow and Wind Fields. *J. Mar. Sci. Eng.* **2023**, *11*, 1710. https://doi.org/10.3390/jmse11091710

Academic Editors: Raul Perianez and Alberto Ribotti

Received: 20 July 2023
Revised: 25 August 2023
Accepted: 25 August 2023
Published: 30 August 2023

1. Introduction

The coastal areas of China have witnessed a flourishing fishing industry, with fish feed playing an indispensable role in marine aquaculture. The development of fisheries heavily relies on the accurate timing and proper placement of fish feed. However, fish feed also introduces various pollutants into the marine ecosystem, including excessive nutrients, antibiotics, and chemical additives [1]. These pollutants can lead to eutrophication, harmful algal blooms, and ecological imbalances in the Yellow Sea [2]. The Yellow Sea region serves as a vital hub for aquaculture production, supplying a considerable portion of the world's seafood [3]. Sustainable aquaculture practices necessitate minimizing the environmental footprint of fish farming, including reducing fish feed pollution. When fish feed pollutants enter the food chain, consumer health can be compromised. Pollutants such as antibiotics and chemical additives may accumulate in fish tissues [4], posing risks to human health upon consumption. Therefore, studying the transport of fish feed in the coastal waters is crucial for better aquaculture management, assessing pollution levels, understanding its impact on water quality, biodiversity, and overall marine ecosystem health, ensuring the safety and quality of seafood, protecting public health, and maintaining consumer confidence in the local aquaculture industry.

In comparison to traditional pollutants, such as oil spills and microplastics, pollution from marine fish feed has received relatively less attention, and its transport and fate are challenging to observe directly. Therefore, numerical simulations of feed transport serve as a valuable reference for damage assessment and emergency response, often being the only available approach in most cases. The feed transport model used in this study is based on the Lagrangian method, which focuses on particles and aims to describe the position evolution of each particle over time. The Lagrangian method was first proposed by Winiarski and Frick [5]. It provides a convenient way to characterize the position and condition of individual particles within the fluid. Early applications of the Lagrangian method primarily focused on oil spills on water surfaces, near-surface, or shallow water environments, such as Fannelop and Sjoen [6], Johansen [7], Elliott [8], Rye [9], Zheng and Yapa [10], and Lonin [11]. Subsequent work aimed at developing enhanced comprehensive oil spill models to describe deepwater spills. Two notable models in this regard are DeepBlow [12] and ADMS/CDOG [13], both capable of simulating the complex behavior of oil spills in deep-sea environments. In recent years, some researchers have applied the Lagrangian method to determine the dynamic growth and transport patterns of floating macroalgae [14,15]. Despite the rapid advancement of remote sensing technologies, the Lagrangian method remains the primary means of studying the transport of spilled oil and floating macroalgae. The main reason is that while remote sensing can effectively estimate oil slick/vegetation coverage and quantify the total amount of oil/algae [16], they cannot capture the entire process due to technological limitations and cloud cover [17]. Additionally, numerical simulations based on the Lagrangian method are often used to study the migration process of microplastics in seawater [18]. This is because numerical simulations are significantly more cost-effective than experimental measurements and on-site observations, and they can predict potential accumulation areas in remote regions where water quality monitoring is not feasible. Although some studies have used Eulerian methods to investigate mixing and dispersion processes in dynamic water systems [19], the transportation and migration of particles still rely on Lagrangian models [20]. In summary, the Lagrangian method has gradually become the mainstream approach for studying the transport and dispersion of various suspended materials in the marine environment.

In this study, we developed a fish feed transport model based on the Lagrangian method, considering the influences of environmental factors, such as temperature and salinity, as well as dynamic factors, including current and wind, within the selected region. With the availability of current and wind data, the model enables the prediction of the transport process of fish feed at different locations and times when released by aquaculture vessels. To prevent the accumulation of pollution due to prolonged fish farming in the same area, we implemented a strategy of changing the farming area every 15 days for aquaculture vessels. Additionally, taking into account the suitable farming temperature for a large yellow croaker (Larimichthys crocea), this study simulated the process of feeding ten times every 15 days within the appropriate farming area from June 15th to November 15th while establishing a reasonable and effective route plan between these dates.

The remainder of this paper is organized as follows. Section 2 presents the main principles of the model, data sources, and the setup of the primary experimental methods. In Section 3, a comprehensive analysis of the results is provided, along with a detailed discussion of the model's prospects. Section 4 focuses on discussing the obtained results and summarizing the key innovations of the model.

2. Model and Methodology

2.1. Model Description

As the commonly accepted view, the transport process of fish feed after its release is generally considered to be controlled by advection and diffusion. The advection–diffusion process of fish feed in seawater is typically described by the following equation:

$$\frac{\partial C}{\partial t} + \vec{V} \cdot \nabla C = \nabla \cdot \left(\vec{K} \cdot \nabla C \right) \quad (1)$$

where C represents the concentration of fish feed in seawater, $\vec{V}$ denotes the velocity vector of advection, ∇ is the gradient operator, $\vec{K}(K_x, K_y, K_z)$ is the diffusion coefficient, and K_x, K_y, and K_z represent the diffusion coefficients in the x, y, and z directions, respectively (m^2/s). It is generally assumed that diffusion in the horizontal direction is isotropic, and the horizontal diffusion coefficients are combined as the horizontal diffusion coefficient, denoted as K_h, such that $K_x = K_y = K_h$.

Equation (1) can be solved using various methods, and in this study, we employed the Lagrangian particle tracking method. This method discretizes the fish feed into a set of particles, with each particle representing a group of feed and being characterized by its spatial coordinates, velocity, diameter, and other relevant attributes. These particles are released at specific positions in the aquatic environment and subsequently subjected to the influences of shear flow, turbulence, and buoyancy, resulting in their movement. The essential properties of the fish feed, such as density and diameter, are integrated into each particle as input parameters for the model, and these characteristics are employed to determine whether the particles float or sink in the water. The advection process of the particles is primarily governed by environmental dynamics, such as ocean currents and wind, which can be simulated using deterministic methods. On the other hand, the diffusion process induced by ocean turbulence is inherently stochastic and is simulated using random motion. By statistically analyzing the positions of all particles, the spatiotemporal distribution of fish feed in the marine environment can be determined.

Simulation of feed transport using the Lagrangian particle tracking method is determined by the following relationships governing the three-dimensional motion of the feed particles:

$$\frac{d\vec{S}}{dt} = \vec{U}_c + \vec{U}_d + \alpha D\vec{U}_w + U_s\vec{k} \tag{2}$$

where $\vec{S} = (x, y, z)$ represents the displacement vector of a feed particle, x and y are the Cartesian coordinates, $\vec{k}$ is the unit vector in the vertical direction, $\vec{U}_c\left(u_{cx}\vec{i}, v_{cy}\vec{j}, u_{cz}\vec{k}\right)$ denotes the velocity of ocean currents, $\vec{U}_d\left(u'\vec{i}, v'\vec{j}, w'\vec{k}\right)$ represents the diffusion velocity during turbulent diffusion, U_s is the settling velocity. U_s is expressed as follows [21,22].

$$U_s = \begin{cases} U_{s,S} & Re_p < 0.2 \\ U_{s,S}\left(1 + 0.15Re_p^{0.687}\right)^{-1} & 0.2 < Re_p < 750 \end{cases} \tag{3}$$

where

$$U_{s,S} = \frac{\left(\rho_w - \rho_f\right)gd^2}{18\mu_w} \tag{4}$$

When $U_s \geq 0$ the particle will float up or suspend in water. Otherwise, it will sink. Where d represents the diameter of the fish feed. $Re_p = U_s\rho_w d/\mu_w$ is the particle Reynolds number [23], ρ_w is the seawater density (1024 kg/m^3), ρ_f is the fish feed density (5×10^2 kg/m^3), and μ_w is the seawater dynamic viscosity (1.01×10^{-3} Pa·s).

The $\alpha D\vec{U}_w$ in Equation (2) represents the wind stress effect, in which $\alpha = 0.03$ is the wind stress coefficient. It should be noted that the wind stress coefficient requires optimization based on further observations. Currently, a temporary reference value of $\alpha = 0.03$ is being used, aligning with the commonly employed coefficient for estimating the transport of oil pollutants affected by wind [24–26]. $\vec{U}_w\left(u_{wx}\vec{i}, u_{wy}\vec{j}\right)$ is the wind vector at a height of 10 m above sea level, and D is the transformation matrix used to calculate the wind deflection angle γ [27].

$$D = \begin{bmatrix} \cos\gamma & \sin\gamma \\ -\sin\gamma & \cos\gamma \end{bmatrix} \tag{5}$$

In this case, when $\left|\vec{U}_w\right| \leq 25\ \text{m/s}$, $\gamma = 40^\circ - 8\sqrt{\left|\vec{U}_w\right|}$, and when $\left|\vec{U}_w\right| > 25\ \text{m/s}$, $\gamma = 0$ [28].

The diffusion velocity $\vec{U}_d\left(u'\vec{i}, v'\vec{j}, w'\vec{k}\right)$ is a random variable, and its components are computed using the random walk method:

$$(u', v', w') = \sqrt{\frac{6}{\Delta t}}\left(R_x\sqrt{K_h}, R_y\sqrt{K_h}, R_z\sqrt{K_z}\right) \tag{6}$$

Here, R_x, R_y, and R_z, are mutually independent, and they are assumed to be uniformly distributed random numbers within the range of -1 to 1. Δt represents the time step. The horizontal diffusion coefficient K_h is computed using the functional form proposed by Pan et al. [29]:

$$K_h = 0.027t^{1.34} \tag{7}$$

The vertical turbulent diffusion coefficient K_z is calculated based on Boufadel et al. [30]:

$$K_z = \left(\frac{\kappa u_*}{0.9}\delta\right)(z + z_0)\left(1 - \frac{z}{MLD}\right) \tag{8}$$

When $z = 0$, the vertical turbulent diffusion coefficient K_z is set to $K_z(z = 0) = \left(\frac{\kappa u_*}{0.9}\delta\right)$, where $\kappa = 0.4$ represents the von-Karman constant, u_* denotes the water friction velocity, and δ is the "enhancement factor" associated with Langmuir circulation, which is assumed to be 1.0 in this study. The MLD stands for the Mixed Layer Depth, defined as the depth at which the temperature is 0.2 °C lower than the sea surface temperature in the current study. z_0 represents the roughness length, which characterizes the surface roughness under the influence of regular waves and can be calculated as follows:

$$z_0 = 1.38 \times 10^{-4} H_s\left(U_w/c_p\right)^{2.66} \tag{9}$$

where H_s represents the significant wave height, $c_p = \frac{gT}{2\pi}$ denotes the wave phase velocity, which is related to the wave period T.

The friction velocity u_* in Equation (5) can be calculated as follows [31]:

$$u_* = \begin{cases} \sqrt{\rho_a C_{d1} U_w (U_w - U_{sur})/\rho_w} & z = 0 \\ \sqrt{\rho_a/\rho_w}\kappa U_w/\ln(10/z_0) & z \neq -H\&z \neq 0 \\ \sqrt{C_{d2} U_{bot}/\rho_w} & z = -H \end{cases} \tag{10}$$

where ρ_a and ρ_w represent air density and water density, respectively. U_{sur} and U_{bot} are the flow velocities at the sea surface and the seabed, respectively. $C_{d1} = 1.13 \times 10^{-3}$ is the drag coefficient at the sea surface, and C_{d2} is the drag coefficient at the seabed, which is computed by matching with a logarithmic boundary layer at height z_{ab} above the seabed.

$$C_{d2} = \max\left[\kappa^2/\ln\left(\frac{z_{ab}}{z_0}\right), 0.0025\right] \tag{11}$$

It is important to note that the density of fish feed may vary depending on its composition and specific formulation. Common types of fish feed, such as pellets or flakes, typically have a density of approximately 267.11–711.35 kg/m^3 [32] and a particle diameter ranging from 1 to 8 mm. In this study, it is essential to acknowledge that certain parameters, such as the diameter and density, were assumed due to the limited availability of direct observations. For the diameter distribution, we employed a normal distribution with a mean value of 4.5 µm and a variance of 1 µm. Regarding the density, we set it to 5×10^2 kg/m^3.

2.2. Hydrodynamic Background Field

The ROMS model generated the velocity and temperature–salinity data used in this study [33,34] and has been extensively validated in previous studies [35–37]. As shown in Figure 1, the model covers the Bohai Sea, Yellow Sea, and East China Sea regions. The horizontal resolution of the model is approximately 1.5 to 2 km; along the continental shelf direction, it ranges from 2 to 3 km, and it gradually increases to about 10 km as it extends towards the open sea. The temporal resolution is 2 h, and the total grid size is 362 × 242, with 20 s-layers in the vertical direction. Wind data and other surface flux data, such as longwave radiation and latent heat flux, are obtained from NCEP with a grid resolution of 0.25° × 0.25° and a temporal resolution of 6 h. The bathymetry data are derived from the ETOPO1 dataset.

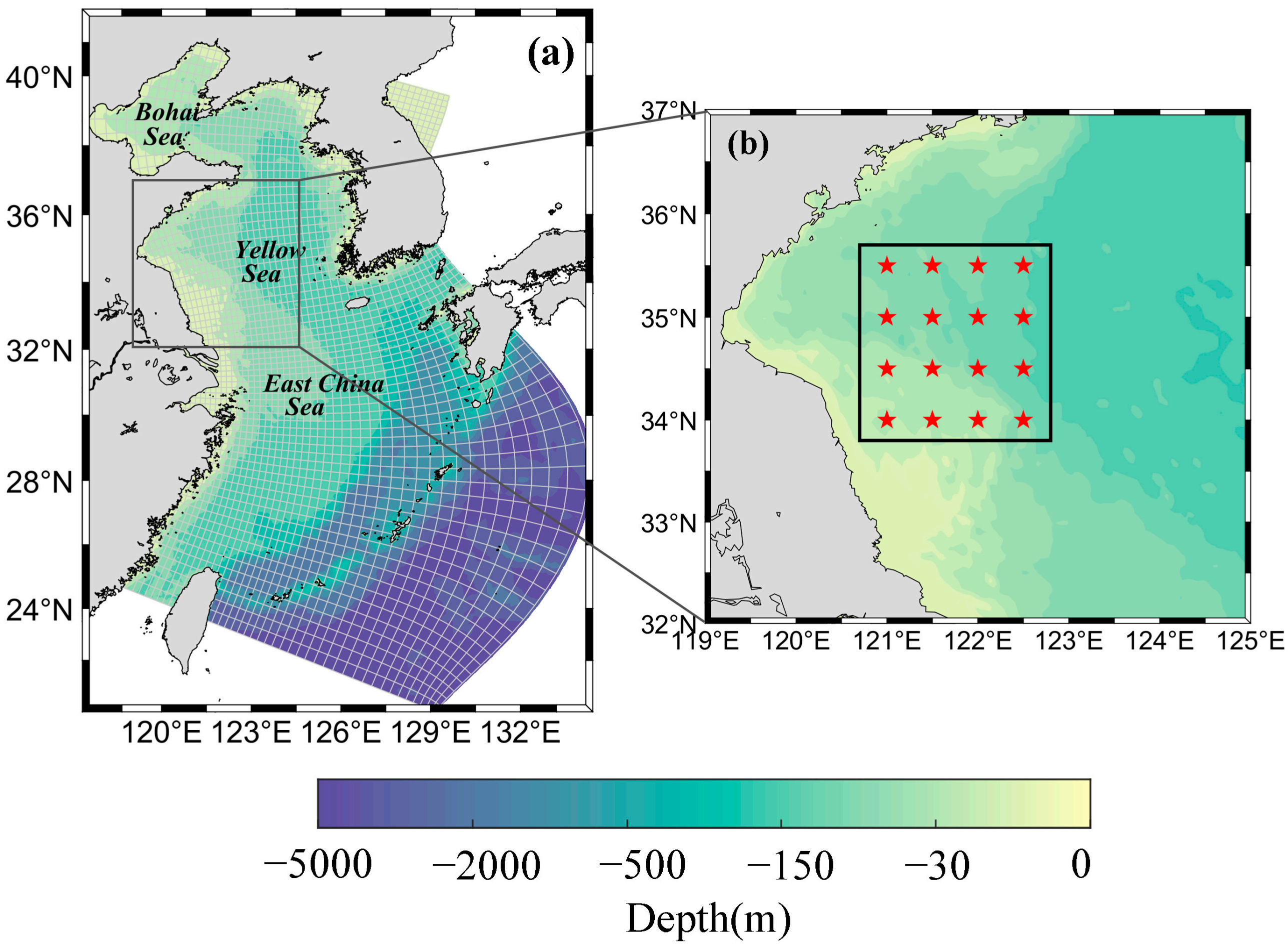

Figure 1. (**a**) ROMS model domain and horizontal curvilinear coordinate system. The total number of grid points is 362 × 242, and the background color represents water depth. (**b**) Specific study area, with red pentagrams indicating the 16 initial particle release locations used for simulation.

The tidal forces at the open boundaries were determined using the TPXO.7.0 global inverse tide model developed by Oregon State University (OSU) [38,39]. The tidal heights are composed of four tidal constituents: M_2, S_2, K_1, and O_1, which explain 90% of the tidal variations in the region. The harmonic constants for each constituent were obtained through linear interpolation of the OSU global tidal model. The open boundary conditions for the barotropic component include the Chapman condition for the surface elevation and the Flather condition for the barotropic velocity [40,41]. The open boundary conditions for the baroclinic component are specified using Orlanski-type radiation conditions [42].

2.3. Experimental Design

To determine the transport trajectory of fish feed under surface winds and ocean currents and understand their contributions to the transport, a series of experiments were designed. In order to meet the requirements of the aquaculture vessel, the designated area shown in Figure 1b was selected as a farming area, and 100,000 particles were each released at 16 locations in the area (Model parameters can be found in Table 1, and the specific 16 locations are listed in Table 2). The model was run for a total duration of 360 h, corresponding to a simulation period of 15 days, to simulate the transport trajectory of fish feed.

Table 1. Model Settings.

Model Parameters	Value
Release depth	0 m
Release duration	15 days
Simulation duration	15 days
Particle quantity	10,000
Particle density	500 kg/m^3

Table 2. Select specific coordinates for 16 locations.

Position	Lon. (°E)	Lat. (°N)	Position	Lon. (°E)	Lat. (°N)
1	121	34	9	121	35
2	121.5	34	10	121.5	35
3	122	34	11	122	35
4	122.5	34	12	122.5	35
5	121	34.5	13	121	35.5
6	121.5	34.5	14	121.5	35.5
7	122	34.5	15	122	35.5
8	122.5	34.5	16	122.5	35.5

In addition to the requirements for the working region aquaculture vessel, the coastal waters of Shandong and Jiangsu provide a conducive environment for aquaculture due to their relatively stable water temperatures, adequate sunlight, and suitable salinity levels. These conditions promote optimal growth and health for the aquaculture of large yellow croaker. Meanwhile, it is generally believed that the optimal temperature for farming large yellow croaker ranges from 18 °C to 28 °C [43]. In order to meet the temperature requirements for fish farming, this study utilized the climatological average temperature field from 2011 to 2021, averaging every half month to obtain the temperature field, as shown in Figures 2 and 3. From Figure 2a, it can be observed that the 18 °C isotherm crosses the selected area during the first half of June, indicating that the temperature in most locations within the study area does not meet the farming requirements. However, during the second half of June, the temperature conditions satisfy the farming requirements, thus setting the model to run from June 16th onwards. Similarly, as shown in Figure 3f, the 18 °C isotherm crosses the selected area during the second half of November, indicating that the temperature in most regions within the study area does not meet the farming requirements. Therefore, the model simulation is terminated on 15 November. Within this defined range, we artificially designed the selection of 16 farming locations to ensure minimal mutual interference between them.

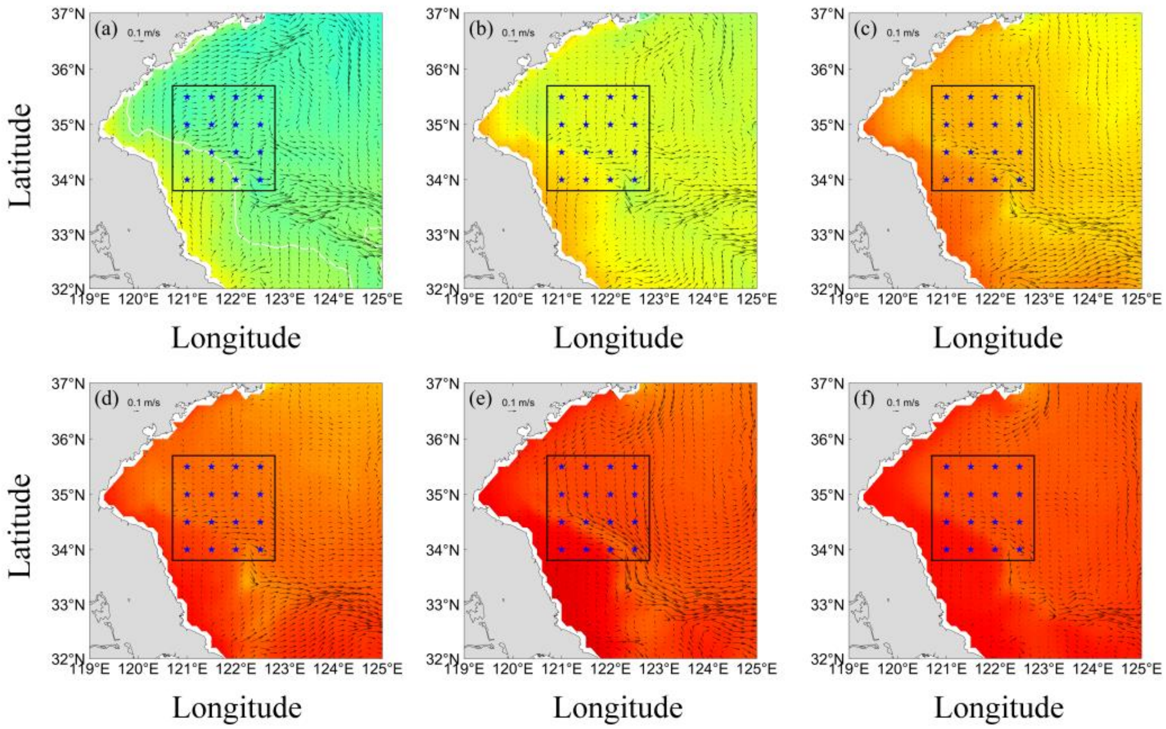

Figure 2. Climatological average distribution of oceanic circulation and temperature from 2011 to 2021 with a 15-day time average: (**a**) 1–15 June, (**b**) 16–30 June, (**c**) 1–15 July, (**d**) 16–31 July, (**e**) 1–15 August, (**f**) 16–31 August. Blue pentagrams indicate the 16 initial release positions used for simulation.

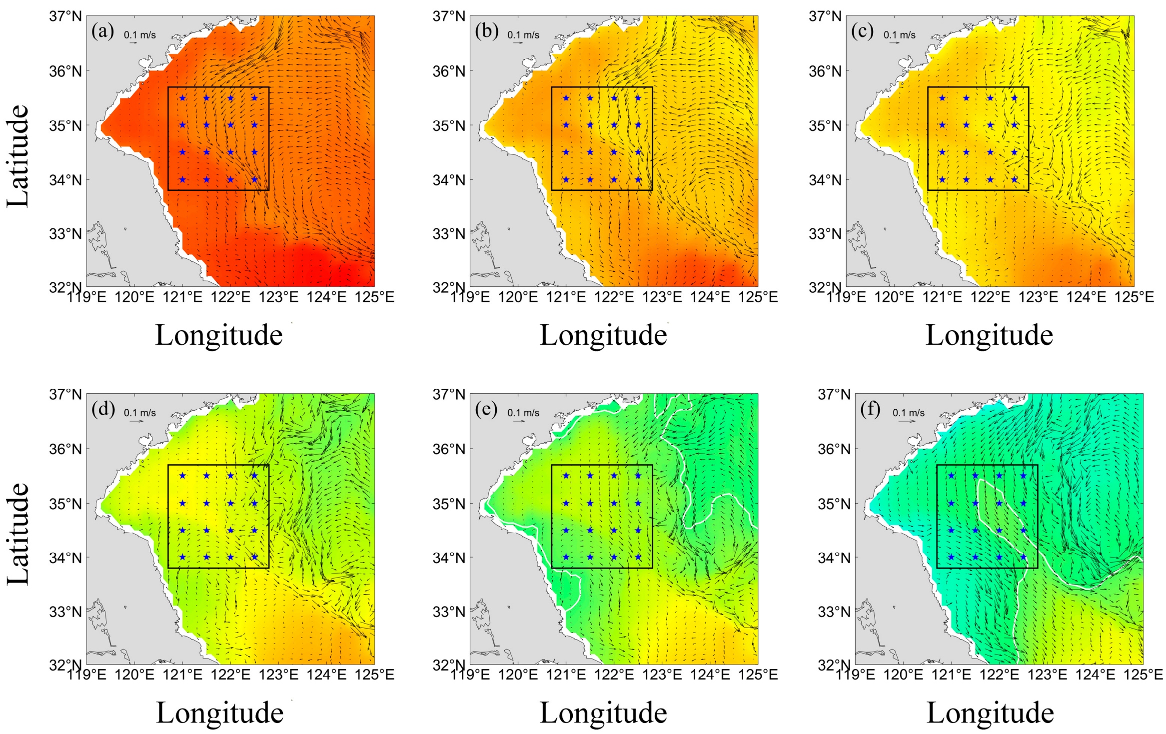

Figure 3. Climatological average distribution of oceanic circulation and temperature from 2011 to 2021 with a 15-day time average: (**a**) 1–15 September, (**b**) 16–30 September, (**c**) 1–15 October, (**d**) 16–31 October, (**e**) 1–15 November, (**f**) 16–30 November. Blue pentagrams indicate the 16 initial release positions used for simulation.

3. Results

3.1. Variability of Environmental Factors

3.1.1. Current

The 15-day average distribution of climatological ocean circulation from 2011 to 2021 is illustrated in Figures 2 and 3. During the latter half of June and July (Figure 2b–d), the coastal surface waters of the Yellow Sea exhibit a northward flow influenced by the EASM, indicating the potential northward drift of particles from their initial release positions. In August (Figure 2e,f), the opposite direction of EASM and southward coastal current (Subei Coastal Current), potentially causing the released particles to remain in the vicinity of the release points without significant transport. Similar patterns can be observed in October. During September, October, and the first half of November (Figure 3a–f), the dominant contribution comes from the EAWM blowing from the north to the south, resulting in a southward drift of particles from their initial release positions. Influenced by ocean currents, there is a high probability of coastal interaction during the southward transport.

3.1.2. Temperature

Due to the specific temperature requirements of large yellow croaker aquaculture, with the optimal range between 18 °C and 28 °C, temperature serves as a crucial physical parameter in this study. The operational time of the model is also strictly guided by the temperature requirements. Figures 2 and 3 also display the climatological average distribution of sea surface temperatures with a 15-day cycle from 2011 to 2021. In the latter half of June, the average sea surface temperature in the Yellow Sea is around 20 °C (Figure 2b), gradually increasing after July (Figure 2c,d) and reaching high temperatures above 25 °C in August (Figure 2e,f). Subsequently, the sea surface temperature starts to decrease (Figure 3a–f).

3.1.3. Wind

Figure 4 shows the climatological average surface wind vectors at 10 m height from 2011 to 2021. Figure 4 shows that from June to July, the coastal waters of the South Yellow Sea are predominantly influenced by southerly and southeast winds, known as East Asia Summer Monsoon (EASM), with an average wind speed of 5 m/s. During the period of EASM, the wind direction is more concentrated in July and more dispersed in June. In the first half of August, the EASM begins to weaken, and the prevailing wind direction shifts to the northeast, while in the latter half of August, the southern winds strengthen. From September to November, when the East Asia Winter Monsoon (EAWM) gradually forms, the prevailing winds begin to change into the west wind and southwest wind.

3.2. Model Results

Figure 5 shows the drift trajectories of the centroids of all released particles after 15 days of simulation for different release dates, including 16 June, 1 July, 16 July, 1 August, 16 August, 1 September, 16 September, 1 October, 16 October, and 1 November. Sixteen initial particle release positions were selected in the nearshore area of the South Yellow Sea (Table 1). The experiments considered the combined effects of sea surface winds and ocean currents.

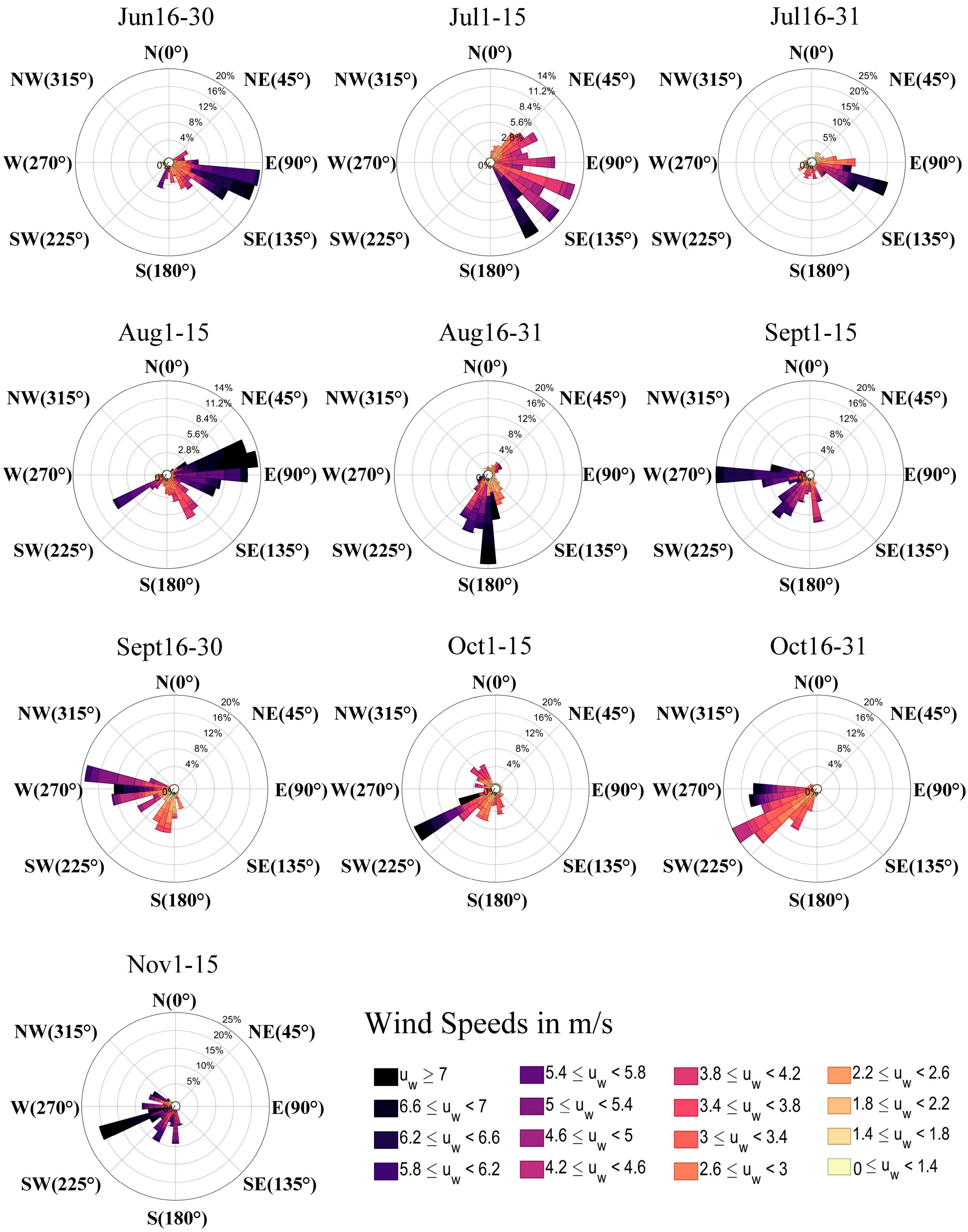

Figure 4. Climatological average surface wind vectors at 10 m height from 2011 to 2021, spatially averaged over a grid of 96 × 156 in the selected area, with a time interval of 6 h.

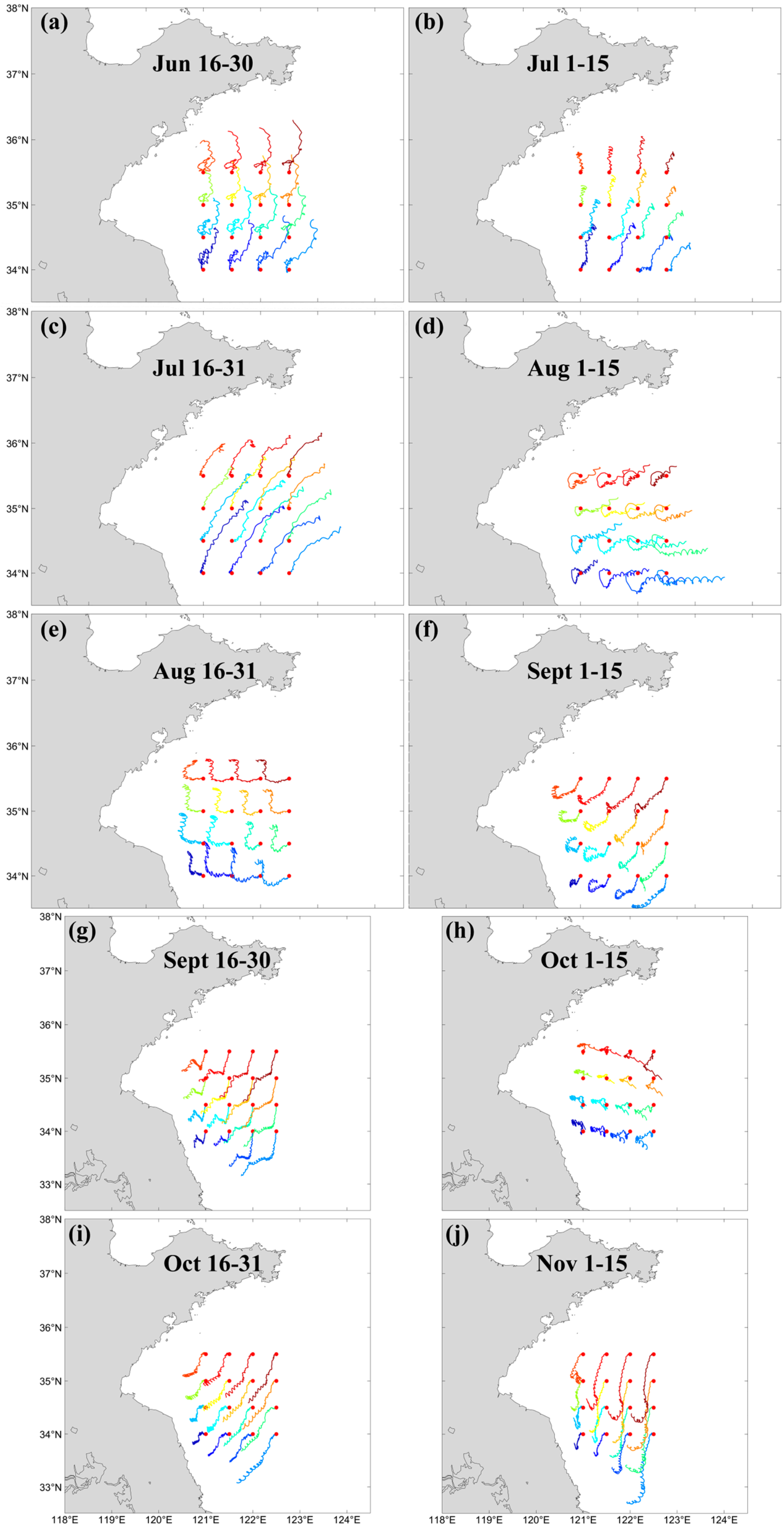

Figure 5. The drift of all particle centroids after 15 days of release at the selected 16 locations for the following initial release dates: (**a**) 16 June, (**b**) 1 July, (**c**) 16 July, (**d**) 1 August, (**e**) 16 August, (**f**) 1 September, (**g**) 16 September, (**h**) 1 October, (**i**) 16 October, and (**j**) 1 November. Each of the 16 colors represents one of the initial release positions.

The results indicate that during the latter half of June, under the influence of southerly and southeasterly winds, the particles exhibit a significant northward drift and then turn towards the northeast direction. The particles released on the right side of the selected region (positions 3, 4, 7, and 8) demonstrate a strong tendency to drift northeastward, which is the combined result of the sea surface winds and ocean currents.

In the first half of July, the particle drift direction is generally similar to that in the latter half of June, moving northward and northeastward under the influence of southerly and southeasterly winds. In the latter half of July, particles released at all 16 selected positions consistently drift toward the northeast direction. It is important to note that during the first half of August and the first half of October, particles form cluster-like distributions around the release points instead of transporting predominantly in a specific direction. This behavior is likely attributed to the weaker flow conditions in August and October, during which the current and wind show opposite directions.

Starting from the second half of August until the first half of November, the particles significantly drift westward and southwestward, which is associated with the influence of the EAWM. Additionally, examining the final positions of all particles after 15 days in the Supplementary Materials reveals that the pollution extent in June, July, and August ranges from 33° N to 37° N and 119° E to 124° E. In September, October, and November, the pollution extent shifts southward, ranging from 31° N to 36° N and 120° E to 124° E, indicating the impact of the EAWM leading to a southern migration of the pollution extent. Furthermore, the model results indicate that particles cannot travel too far in a short period, and there are spiral oscillations caused by rotary tidal currents near the release points.

In summary, with the known surface winds and ocean currents, it is possible to determine the specific drift direction of the particles and their spatial extent by model simulation.

3.3. Empirical Relationship

3.3.1. Quantitative Analysis

In this study, 100,000 particles were released in the selected area of the Yellow Sea to simulate the transport of fish feed. After 15 days, the transport of the feed varies in terms of trajectory and spatial extent, depending on the release time and location. However, regardless of the extent of transport, the centroid position of the feed can be determined. Using the centroid position as the reference, characteristic circles were defined with particles containing different percentages (100%, 90%, 80%, 70%, and 60%). The radius of each circle, as well as the average current velocity and direction within the circle, were calculated. As an example, Table 3 presents the properties of circles corresponding to different percentages of particles after 15 days of transport from the release point on 16 June at position (34° N, 121° E). The distribution range of different percentages of particle quantities after 15 days is shown in Figure 6.

Table 3. Properties of particles released on 16 June at point (34° N, 121° E) in different percentage feature circles.

Percentage	100%	90%	80%	70%	60%
Radius R (km)	84.98	57.33	43.81	39.10	35.40
Average flow velocity (m/s)	0.026	0.029	0.033	0.033	0.036
Average flow direction (°)	94.40	87.89	83.99	83.76	81.73

From Table 3, it can be observed that the maximum difference in average current velocity within the circles of different percentage ranges is 0.01 m/s and the maximum difference in average current direction is 12.67 degrees.

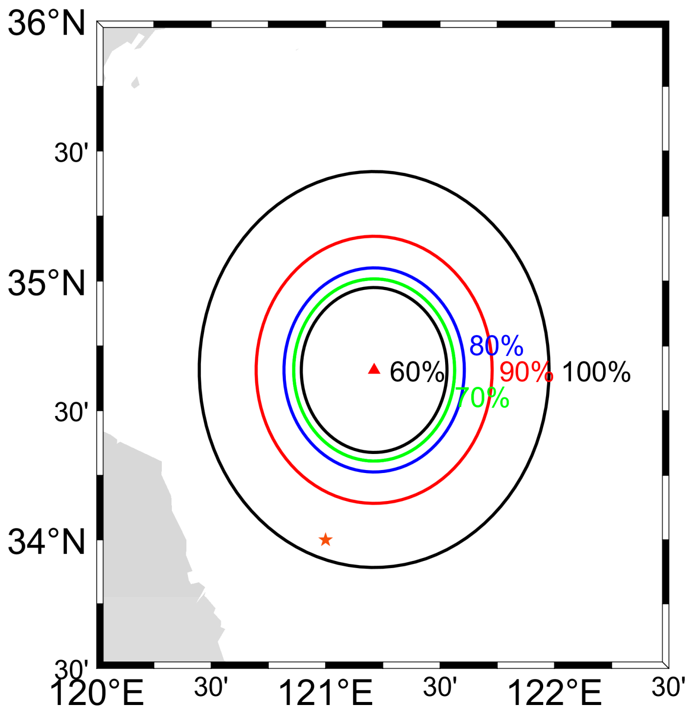

Figure 6. The distribution range of different percentages of particle quantities after 15 days of advection from the release of 100,000 particles on 16 June at location (34° N, 121° E). The red pentagram represents the initial release position, and the red triangle represents the centroid.

To further establish the relationship between the simulation and the dynamics in a characteristic circle, the difference between simulated transport and the transport using combined current and wind are analyzed. The direction of the line connecting the initial position and the centroid is referred to as Direction 1. The combined current and wind direction within the circles for different percentages of particle quantities is considered Direction 2. By comparing Direction 1 and Direction 2, an accurate angle difference θ can be obtained, as shown in Table 4. The distance between the initial position and the centroid is defined as Distance 1, while the product of the average current speed within the circles for different particle quantities and the model running time of 15 days is defined as Distance 2. The ratio β of Distance 2 to Distance 1 serves as an important reference for estimating the distance traveled by the particles. The comparison results are presented in Table 5.

Table 4. Comparison between Direction 1 and Direction 2.

Percentage	100%	90%	80%	70%	60%
Direction 1 (°)	75.01	75.01	75.01	75.01	75.01
Direction 2 (°)	94.40	87.89	83.99	83.76	81.73
Angle difference θ	19.39	12.88	8.98	8.75	6.72

Table 5. Comparison between Distance 1 and Distance 2.

Percentage	100%	90%	80%	70%	60%
Distance 1 (km)	75.60	75.60	75.60	75.60	75.60
Distance 2 (km)	139.21	142.33	148.07	148.54	151.92
Distance Ratio β	1.84	1.88	1.96	1.96	2.01

The results in Tables 4 and 5 are only representative of one case with the release time on 16 June and the initial release position at (34° N, 121° E), and they do not represent the overall trend. Therefore, the calculations described above were performed for a total of 10 sets of experiments, each consisting of 16 scenarios, resulting in a total of 160 scenarios. Specifically, the calculations were conducted for the centroid position, radius, combined current and wind, Direction 1, Direction 2, Distance 1, Distance 2, angle difference θ, and distance ratio β for each of the 160 scenarios after 15 days of particle release and advection. The average angle difference θ and distance ratio β were then calculated based on the results of the 160 scenarios, as shown in Figure 7.

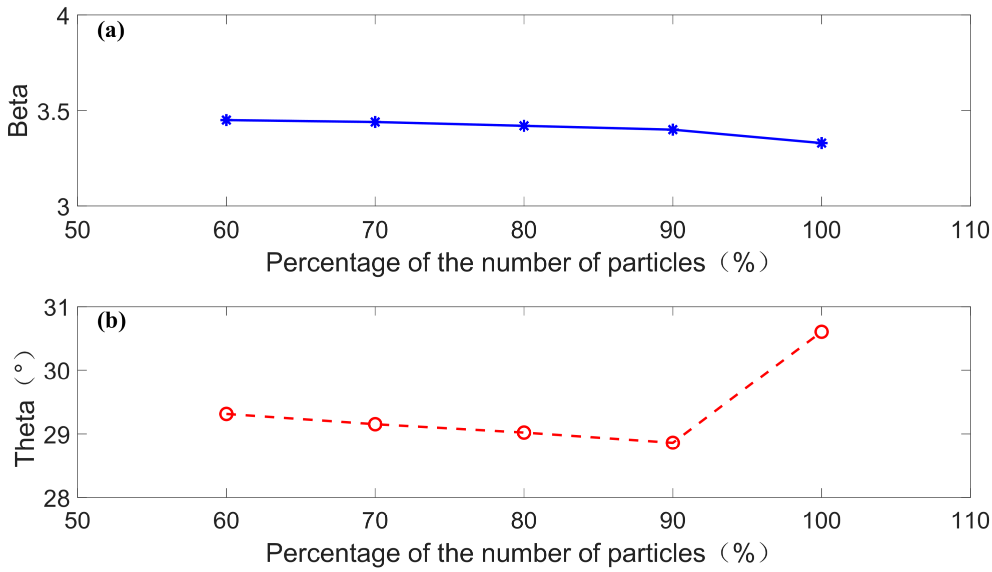

Figure 7. (**a**) Average distance ratio β and (**b**) Average angle difference θ for the 160 cases with particle percentages of 100%, 90%, 80%, 70%, and 60% of the total particles.

The results indicate that there is little variation in the distance ratio β for particle percentages of 100%, 90%, 80%, 70%, and 60%, which range from 3.3 to 3.5. This suggests that regardless of the initial release position chosen for the particles, the distance traveled by the particles can be reasonably estimated given the known surface winds and ocean currents. Furthermore, the angle difference θ ranges from 28.9 to 30.6 degrees, allowing for a reasonable estimation of the particle movement direction. It is noteworthy that the average angle difference is minimized at 28.9 degrees when the particle percentage is 90% of the total, indicating that the characteristic circle containing 90% of the particles can be considered the optimal characteristic circle. The maximum angle difference occurs when the particle percentage is 100% of the total.

3.3.2. Derivation of Formulas

Based on the quantitative analysis above, under the knowledge of sea surface winds and ocean currents, for a given percentage of particles, a characteristic circle can be defined to contain these particles. By calculating the combined current and wind velocity within this area, the displacement distance $\vec{d}(dx, dy)$ from the initial position to the centroid of the particles after a certain period can be obtained. The specific empirical formula is as follows:

$$\begin{aligned} dx &= \tfrac{1}{\beta} T(u_a \cos\theta - v_a \sin\theta) \\ dy &= \tfrac{1}{\beta} T(u_a \sin\theta + v_a \cos\theta) \end{aligned} \tag{12}$$

where β is the distance ratio mentioned in Section 3.3.1, and its optimal solution can be obtained through fitting. T represents the model running time, and $\vec{U_e}(u_e, v_e)$ represents the equivalent velocity of the current and wind fields within the characteristic circle containing 90% of the particles, as expressed in Equation (13).

$$\vec{U}_e(u_e, v_e) = \vec{U}_c(u_c, v_c) + \alpha D\vec{U}_w(u_w, v_w) \tag{13}$$

where θ represents the angle difference, and D is the transformation matrix (expression given in Section 2.1). Substituting Equation (13) into Equation (12), we have:

$$\begin{aligned} dx &= \frac{1}{\beta}T[A\cos\theta - B\sin\theta] \\ dy &= \frac{1}{\beta}T[A\sin\theta + B\cos\theta] \end{aligned} \tag{14}$$

where the expressions for A and B are given by Equation (15).

$$\begin{aligned} A &= u_c + \alpha u_w \cos\gamma + \alpha v_w \sin\gamma \\ B &= v_c - \alpha u_w \sin\gamma + \alpha v_w \cos\gamma \end{aligned} \tag{15}$$

Applying the 160 sets of cases in Section 3.3.1 to Equation (14) using the least squares method, we can solve for the optimal values of β and θ. Thus, we aim to solve for:

$$\begin{cases} \min\limits_{\beta,\theta} \sum\limits_{i=1}^{160} \left\{ dx_i - \frac{1}{\beta}T[A\cos\theta - B\sin\theta] \right\}^2 \\ \min\limits_{\beta,\theta} \sum\limits_{i=1}^{160} \left\{ dy_i - \frac{1}{\beta}T[A\sin\theta + B\cos\theta] \right\}^2 \end{cases} \tag{16}$$

The optimal coefficients are obtained as β = 3.36 and θ = 29.2°. These values are then used as the basis for designing the navigation routes of aquaculture vessels by substituting them into Equation (14).

3.4. Design of Aquaculture Vessel Navigation Routes

Based on the above study, with the understanding of the specific displacement and direction of fish feed after a certain period of time, and considering the fact that fish feed can transform into pollutants over time, it is possible to design a rational route that can effectively avoid the spread of pollutants.

On June 16th, when (121° E, 34° N) is chosen as the initial release position, according to the empirical formula, the fish feed particles are projected to move in a direction of approximately 75° east-northeast. Considering the avoidance of pollutant drift, the fishing vessel is designed to travel eastward within the selected area after 15 days. On 1 July, when the fishing vessel reaches (121.5° E, 34° N), the empirical formula indicates that the pollutant is still primarily drifting northward before turning northeast after 15 days. Therefore, the route is designed for the fishing vessel to travel eastward. On 16 July, when the fishing vessel reaches (122° E, 34° N), the empirical formula suggests that the pollutant will primarily move in a northeast direction after 15 days. Therefore, the route is designed for the fishing vessel to travel northward.

Based on the numerical modeling results, the fishing vessel will travel northward twice in August, eastward at the beginning of September, southward three times from mid-September to the end of October, and westward in early November. This results in the design of the routes for each month that satisfy the temperature requirements for the cultivation of yellow croaker, as shown in Figure 8.

Comparison with the model results reveals a close agreement between the predicted pollutant drift paths using the empirical formula. This demonstrates that the empirical formula can effectively predict the pollutant drift path of fish feed, thereby aiding in the optimization of computational resource utilization within the study area.

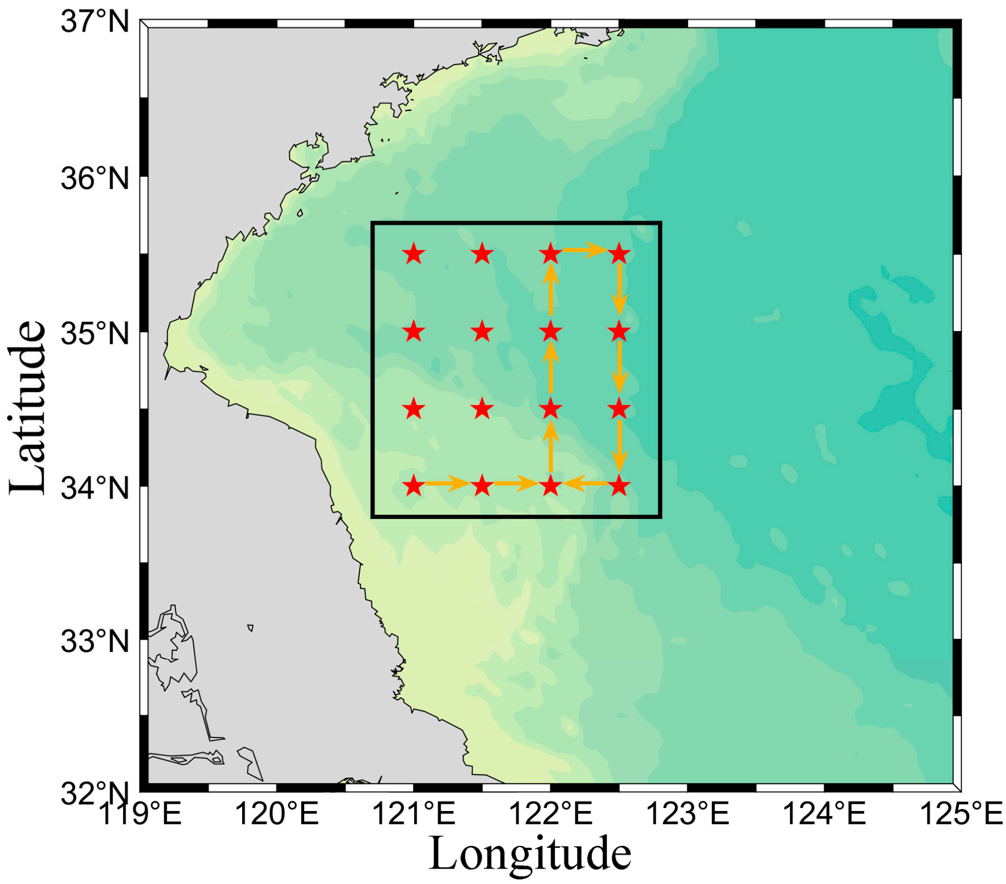

Figure 8. Route design map. The orange lines represent the navigation routes, while the red pentagrams indicate the 16 initial release positions as part of the experimental design. The background colors correspond to different water depths.

3.5. Prospects on Model Development

Currently, there is limited use of Lagrangian particle tracking to study the transport of fish feed, with most marine pollution research focusing on topics like oil spills, microplastics, and large floating algae. Our study provides a new direction for the rational utilization of fisheries resources and the optimal planning of aquaculture vessel routes.

Different locations exhibit significant variations in ocean currents and surface winds. By employing the Lagrangian particle tracking method, each particle is treated as an independent simulation unit, incorporating critical environmental factors, such as ocean currents, surface winds, and temperature, relevant to fish farming. This enables us to obtain essential information, such as equivalent current velocity and direction, in an equivalent circles model.

In the model, the fish feed is treated as Lagrange particles; however, it is essential to acknowledge the potential biochemical reactions it may undergo. Furthermore, fisheries density will significantly influence the distribution of fish feed, as fish consumption and swimming patterns disturb the localized feed dispersion. Thus, the transport range of fish feed in reality may be smaller than in the model simulation. To achieve a more accurate representation of its transport processes, future research should incorporate fisheries density data and integrate the chemical interactions and transformations of fish feed. Additionally, it should be noted that in our study, fish feed is floated on the water surface based on certain parameters. Nevertheless, various factors, including waves and water absorption of feed, can also cause fish feed to sink. Another point worth noting is that the wind stress coefficient α of 0.03 in the model is based on the transport of oil pollutants affected by wind, while there might be differences between the transport characteristics of oil and fish feed. To gain a more comprehensive understanding of the dynamic state changes of fish feed, further research should explore multiple factors and improve parameter configuration to better comprehend the dynamic state changes of fish feed.

4. Summary and Conclusions

This study utilizes the Lagrangian particle tracking method to develop a transport model for fish feed. Numerical experiments are conducted in the nearshore waters of the Yellow Sea to investigate the impact of surface winds and ocean currents on the transport of fish feed. The model combines the effects of ocean currents and surface winds on pollutant transport and employs a series of numerical experiments to simulate the drift of pollutants. Considering the temperature requirements in aquaculture conditions, the sea surface temperature is set as an important influencing factor.

Based on a series of numerical experiments, this study determines characteristic circles that represent the distribution pattern of pollutants. These circles represent circular regions containing different percentages of particles relative to the total number of particles. The study calculates the radius of the circle, the centroid of particles within the circle, and the combined current and wind velocity within the circle. Additionally, the study quantitatively analyzes the angular difference between the direction of the line connecting the initial position and the mass center and the average current direction. It also examines the distance ratio between the line connecting the initial position and the mass center and the average current velocity multiplied by the running time. The results indicate that the angular difference θ ranges from 28.9° to 30.6°, allowing for reasonable calculation of particle movement direction. When the particle count accounts for 90% of the total particles, the average angular difference is minimal at 28.9°, and the equivalent circle containing 90% of the particles is considered the optimal equivalent circle. The distance ratios β for particle counts representing 100%, 90%, 80%, 70%, and 60% of the total particles show little difference, ranging from 3.3 to 3.5.

Based on the information on flow fields and wind fields within the characteristic circles, we derived an empirical formula to describe the distribution of pollutants. In the process of obtaining the empirical formula, we used the method of least squares to fit the test cases and determine the optimal values of β and θ. The empirical formula enables us to predict the specific direction of particle drift and the distance after a certain period of time using the data of flow fields and wind fields within the characteristic circles. Furthermore, as fish feed itself can also contribute to marine pollution, the empirical formula can be utilized to design an effective route that avoids pollution. This approach not only optimizes the utilization of computational resources within the study area but also aids in the rational planning of routes for aquaculture vessels.

However, the model still has some limitations. The model treats fish feed as Lagrange particles, but it's important to note potential biochemical reactions. Moreover, fisheries density significantly impacts feed distribution, as fish feeding and swimming patterns disrupt localized dispersion. Additionally, we assumed that feed floats on the water surface based on certain parameters, ignoring factors that may cause it to sink, such as waves and density change due to water absorption of feed. Another point worth noting is that the wind stress coefficient α of 0.03 is oil-based and might differ from feed behavior. Limited by observational data, we plan to conduct further observations to address the aforementioned limitations and improve the quality of our study. By utilizing observational data, we can optimize the model's parameters and enhance its reliability. Overall, our research provides valuable insights into the understanding of the drift behavior of fish feed pollutants in the Yellow Sea. The establishment of the empirical formula and the design of pollution-avoiding routes contribute to effective pollution management and the planning of marine activities in the region.

Supplementary Materials: The following supporting information can be downloaded at: https://www.mdpi.com/article/10.3390/jmse11091710/s1, Figures S1–S40: Particle distribution after 15 days of model run. Red dots represent the initial release points on June 16th at positions 1, 2, 5, and 6, while black dots indicate particle positions after a 15-day model simulation.

Author Contributions: N.W., conceptualization, data curation, formal analysis, investigation, methodology, software, validation, visualization, writing—original draft, and writing—review and editing; R.C., conceptualization, software, methodology, writing—review and editing, and investigation; H.S., conceptualization, funding acquisition, methodology, project administration, and resources; X.L., formal analysis, methodology, project administration, and resources. All authors have read and agreed to the published version of the manuscript.

Funding: This research was supported by the Key R&D Program of Shandong Province (S & T Demonstration Project) (No. 2021SFGC0701) and the National Natural Science Foundation of China (No. 2006210).

Institutional Review Board Statement: Not applicable.

Informed Consent Statement: Not applicable.

Data Availability Statement: Data will be made available on request.

Acknowledgments: Rushui Xiao, Shengyi Jiao, Junting Guo, and Yuzhe Wang participated in the discussion on the study method and manuscript preparation with useful suggestions.

Conflicts of Interest: The authors declare no conflict of interest.

References

1. Cabello, F.C.; Godfrey, H.P.; Tomova, A.; Ivanova, L.; Doelz, H.; Millanao, A.; Buschmann, A.H. Antimicrobial Use in Aquaculture Re-Examined: Its Relevance to antimicrobial Resistance and to Animal and Human Health. *Environ. Microbiol.* **2013**, *15*, 1917–1942. [CrossRef] [PubMed]
2. Liu, X.; Lu, S.; Guo, W.; Xi, B.; Wang, W. Antibiotics in the Aquatic Environments: A Review of Lakes, China. *Sci. Total Environ.* **2018**, *627*, 1195–1208. [CrossRef]
3. Xu, J.; Han, L.; Yin, W. Research on the Ecologicalization Efficiency of Mariculture Industry in China and Its Influencing Factors. *Mar. Policy* **2022**, *137*, 104935. [CrossRef]
4. Schrenk, D.; Bignami, M.; Bodin, L.; Chipman, J.K.; del Mazo, J.; Grasl-Kraupp, B.; Hogstrand, C.; Hoogenboom, L.; Leblanc, J.-C.; Nebbia, C.S.; et al. Risk to Human Health Related to the Presence of Perfluoroalkyl in Food. *EFSA J.* **2020**, *18*, e06223. [CrossRef] [PubMed]
5. Winiarski, L.D.; Frick, W.F. *Cooling Tower Plume Model*; US Environmental Protection Agency, Office of Research and Development: Washington, DC, USA, 1976.
6. Fannelop, T.; Sjoen, K. Hydrodynamics of Underwater Blowouts. In Proceedings of the 18th Aerospace Sciences Meeting, Pasadena, CA, USA, 14–16 January 1980; p. 219.
7. Johansen, Ø. The Halten Bank Experiment-Observations and Model Studies of Drift and Fate of Oil in the Marine Environment. In Proceedings of the 11th Arctic Marine Oil Spill Program (AMOP) Techn. Seminar. Environment Canada, Ottawa, ON, Canada, June 1984; pp. 18–36.
8. Elliott, A.J. Shear Diffusion and the Spread of Oil in the Surface Layers of the North Sea. *Dtsch. Hydrogr. Z.* **1986**, *39*, 113–137. [CrossRef]
9. Rye, H. Model for Calculation of Underwater Blow-out Plume. In Proceedings of the Arctic and Marine Oilspill Program Technical Seminar; Ministry of Supply and Services, Edmonton, AB, Canada, 8–10 June 1994; p. 849.
10. Zheng, L.; Yapa, P.D. Simulation of Oil Spills from Underwater Accidents II: Model Verification. *J. Hydraul. Res.* **1998**, *36*, 117–134. [CrossRef]
11. Lonin, S.A. Lagrangian Model for Oil Spill Diffusion at Sea. *Spill Sci. Technol. Bull.* **1999**, *5*, 331–336. [CrossRef]
12. Johansen, Ø. DeepBlow–a Lagrangian Plume Model for Deep Water Blowouts. *Spill Sci. Technol. Bull.* **2000**, *6*, 103–111. [CrossRef]
13. Zheng, L.; Yapa, P.D. Modeling Gas Dissolution in Deepwater Oil/Gas Spills. *J. Mar. Syst.* **2002**, *31*, 299–309. [CrossRef]
14. Lee, J.H.; Pang, I.; Moon, I.; Ryu, J. On Physical Factors That Controlled the Massive Green Tide Occurrence along the Southern Coast of the Shandong Peninsula in 2008: A Numerical Study Using a Particle-tracking Experiment. *J. Geophys. Res. Ocean.* **2011**, *116*, C12036. [CrossRef]
15. Putman, N.F.; Goni, G.J.; Gramer, L.J.; Hu, C.; Johns, E.M.; Trinanes, J.; Wang, M. Simulating Transport Pathways of Pelagic Sargassum from the Equatorial Atlantic into the Caribbean Sea. *Prog. Oceanogr.* **2018**, *165*, 205–214. [CrossRef]
16. Wang, M.; Hu, C. Mapping and Quantifying Sargassum Distribution and Coverage in the Central West Atlantic Using MODIS Observations. *Remote Sens. Environ.* **2016**, *183*, 350–367. [CrossRef]
17. Keesing, J.K.; Liu, D.; Fearns, P.; Garcia, R. Inter-and Intra-Annual Patterns of Ulva Prolifera Green Tides in the Yellow Sea during 2007–2009, Their Origin and Relationship to the Expansion of Coastal Seaweed Aquaculture in China. *Mar. Pollut. Bull.* **2011**, *62*, 1169–1182. [CrossRef]
18. Jalón-Rojas, I.; Wang, X.H.; Fredj, E. A 3D Numerical Model to Track Marine Plastic Debris (TrackMPD): Sensitivity of Microplastic Trajectories and Fates to Particle Dynamical Properties and Physical Processes. *Mar. Pollut. Bull.* **2019**, *141*, 256–272. [CrossRef] [PubMed]

19. Alosairi, Y.; Alsulaiman, N. Hydro-Environmental Processes Governing the Formation of Hypoxic Parcels in an Inverse Estuarine Water Body: Model Validation and Discussion. *Mar. Pollut. Bull.* **2019**, *144*, 92–104. [CrossRef] [PubMed]
20. Van Utenhove, E. Modelling the Transport and Fate of Buoyant Macroplastics in Coastal Waters. Master's Thesis, Delft University of Technology, Delft, The Netherland, December 2019.
21. Aiyer, A.K.; Yang, D.; Chamecki, M.; Meneveau, C. A Population Balance Model for Large Eddy Simulation of Polydisperse Droplet Evolution. *J. Fluid. Mech.* **2019**, *878*, 700–739. [CrossRef]
22. Cao, R.; Chen, H.; Li, H.; Fu, H.; Wang, Y.; Bao, M.; Tuo, W.; Lv, X. A Mesoscale Assessment of Sinking Oil during Dispersant Treatment. *Ocean. Eng.* **2022**, *263*, 112341. [CrossRef]
23. Cui, F.; Boufadel, M.C.; Geng, X.; Gao, F.; Zhao, L.; King, T.; Lee, K. Oil Droplets Transport under a Deep-water Plunging Breaker: Impact of Droplet Inertia. *J. Geophys. Res. Ocean.* **2018**, *123*, 9082–9100. [CrossRef]
24. Stolzenbach, K.D.; Madsen, O.S.; Adams, E.E.; Pollack, A.M.; Cooper, C. *A Review and Evaluation of Basic Techniques for Predicting the Behavior of Surface Oil Slicks*; Report (Massachusetts Institute of Technology. Sea Grant Program), no. MITSG 77-8; Massachusetts Institute of Technology: Cambridge, MA, USA, 1977.
25. Wang, S.D.; Shen, Y.M.; Zheng, Y.H. Two-Dimensional Numerical Simulation for Transport and Fate of Oil Spills in Seas. *Ocean. Eng.* **2005**, *32*, 1556–1571. [CrossRef]
26. Li, Y.; Chen, H.; Lv, X. Impact of Error in Ocean Dynamical Background, on the Transport of Underwater Spilled Oil. *Ocean. Model* **2018**, *132*, 30–45. [CrossRef]
27. Samuels, W.B.; Huang, N.E.; Amstutz, D.E. An Oilspill Trajectory Analysis Model with a Variable Wind Deflection Angle. *Ocean. Eng.* **1982**, *9*, 347–360. [CrossRef]
28. Wang, J.; Shen, Y. Modeling Oil Spills Transportation in Seas Based on Unstructured Grid, Finite-Volume, Wave-Ocean Model. *Ocean. Model* **2010**, *35*, 332–344. [CrossRef]
29. Pan, Q.; Yu, H.; Daling, P.S.; Zhang, Y.; Reed, M.; Wang, Z.; Li, Y.; Wang, X.; Wu, L.; Zhang, Z. Fate and Behavior of Sanchi Oil Spill Transported by the Kuroshio during January–February 2018. *Mar. Pollut. Bull.* **2020**, *152*, 110917. [CrossRef]
30. Boufadel, M.; Liu, R.; Zhao, L.; Lu, Y.; Özgökmen, T.; Nedwed, T.; Lee, K. Transport of Oil Droplets in the Upper Ocean: Impact of the Eddy Diffusivity. *J. Geophys. Res. Oceans* **2020**, *125*, e2019JC015727. [CrossRef]
31. Bandara, U.C.; Yapa, P.D. Bubble Sizes, Breakup, and Coalescence in Deepwater Gas/Oil Plumes. *J. Hydraul. Eng.* **2011**, *137*, 729–738. [CrossRef]
32. Khater, E.-S.G.; Bahnasawy, A.H.; Ali, S.A. Physical and Mechanical Properties of Fish Feed Pellets. *J. Food Process Technol.* **2014**, *5*, 1.
33. Haidvogel, D.B.; Blanton, J.; Kindle, J.C.; Lynch, D.R. Coastal Ocean Modeling: Processes and Real-Time Systems. *Oceanography* **2000**, *13*, 35–46. [CrossRef]
34. Shchepetkin, A.F.; McWilliams, J.C. The Regional Oceanic Modeling System (ROMS): A Split-Explicit, Free-Surface, Topography-Following-Coordinate Oceanic Model. *Ocean. Model* **2005**, *9*, 347–404. [CrossRef]
35. Li, M.; Rong, Z. Effects of Tides on Freshwater and Volume Transports in the Changjiang River Plume. *J. Geophys. Res. Ocean.* **2012**, *117*. [CrossRef]
36. Cao, R.; Chen, H.; Rong, Z.; Lv, X. Impact of Ocean Waves on Transport of Underwater Spilled Oil in the Bohai Sea. *Mar. Pollut. Bull.* **2021**, *171*, 112702. [CrossRef]
37. Rong, Z.; Li, M. Tidal Effects on the Bulge Region of Changjiang River Plume. *Estuar. Coast. Shelf Sci.* **2012**, *97*, 149–160. [CrossRef]
38. Egbert, G.D.; Bennett, A.F.; Foreman, M.G.G. TOPEX/POSEIDON Tides Estimated Using a Global Inverse Model. *J. Geophys. Res. Ocean.* **1994**, *99*, 24821–24852. [CrossRef]
39. Egbert, G.D.; Erofeeva, S.Y. Efficient Inverse Modeling of Barotropic Ocean Tides. *J. Atmos. Ocean. Technol.* **2002**, *19*, 183–204. [CrossRef]
40. Chapman, D.C. Numerical Treatment of Cross-Shelf Open Boundaries in a Barotropic Coastal Ocean Model. *J. Phys. Oceanogr.* **1985**, *15*, 1060–1075. [CrossRef]
41. Flather, R.A. A Tidal Model of the Northwest European Continental Shelf. *Mem. Soc. Roy. Sci. Liege* **1976**, *10*, 141–164.
42. Orlanski, I. A Simple Boundary Condition for Unbounded Hyperbolic Flows. *J. Comput. Phys.* **1976**, *21*, 251–269. [CrossRef]
43. Chen, Y.; Huang, W.; Shan, X.; Chen, J.; Weng, H.; Yang, T.; Wang, H. Growth Characteristics of Cage-Cultured Large Yellow Croaker Larimichthys Crocea. *Aquac. Rep.* **2020**, *16*, 100242. [CrossRef]